

## MODELING OF STRAIN LOCALIZATION FOR THE GURSON-TVERGAARD-NEEDLEMAN PLASTICITY MODEL USING STRONG DISCONTINUITY MODES.

Sebastián D' hers<sup>a</sup> and Eduardo N. Dvorkin<sup>b,c</sup>

<sup>a</sup> *Laboratorio de Mecánica Computacional, Instituto Tecnológico de Buenos Aires, Av. E. Madero 399, C1106ACD, Buenos Aires, Argentina. [sdhers@itba.edu.ar](mailto:sdhers@itba.edu.ar), <http://www.itba.edu.ar>*

<sup>b</sup> *Facultad de Ingeniería, Universidad de Buenos Aires, Av. Las Heras 2214, C1127AAR, Buenos Aires, Argentina, <http://www.fi.uba.ar>*

<sup>c</sup> *Sim & Tec, Pueyrredón 2130, C1119ACR, Buenos Aires, Argentina, [edvorkin@simytec.com](mailto:edvorkin@simytec.com), <http://www.simytec.com>*

**Keywords:** Plasticity, strain localization, shear band, strong discontinuity, multiple scales, Gurson-Tvergaard-Needleman model.

**Abstract.** The Gurson-Tvergaard-Needleman material model is frequently used to model ductile failure. At the inception of ductile fracture, the modeling of the strain localization phenomenon requires the use of different scales for the description of the continuum and the localized subdomains, thus inducing mesh dependent results when finite elements are used.

In this work the necessary and sufficient localization conditions are explored for the Gurson-Tvergaard-Needleman material and the outcome is inserted into a mesh indifferent formulation with the use of embedded strong discontinuity modes. An heuristic rule to set a proper interscales connection between the localized and the continuum scales is introduced. The new formulation does not require a specific mesh refinement to model strain localization and provides mesh independent results.

## 1 INTRODUCTION

Ductile fracture is a complex phenomenon normally preceded by a strong plastic deformation localized in a very narrow zone. The mechanical process that triggers this deformation concentration is the strain localization, see [Rice \(1976\)](#) and [Ottosen and Runesson \(1991\)](#). The typical band width of this localization is much smaller than the problem domain dimensions; with the material inside the band undergoing a strong degradation process and the off-band material undergoing a less severe degradation process. Thus a multiscale formulation is required to assess the simultaneous modeling of the localized plastic deformations and of the elastoplastic continua.

To describe the ductile material behavior we adopt the Gurson-Tvergaard-Needleman (G-T-N) material model. G-T-N material model is used to model the material mechanical degradation in void containing ductile materials. The plasticity model was introduced in [Gurson \(1975\)](#) and [Gurson \(1977\)](#), and modified in [Tvergaard \(1981\)](#), [Tvergaard \(1982\)](#) and [Tvergaard and Needleman \(1984\)](#). It incorporates to the standard  $J_2$  plasticity model the material degradation that is due to the nucleation, growth and coalescence of voids.

We summarize some of the techniques that have been proposed for dealing with the multiple coexisting scales in shear banding of ductile materials. The enhancement of the strain fields used in the finite element formulation was discussed in [Ortiz et al. \(1987\)](#), where a strain jump function was added to each element where the localization criterion was satisfied. Different enhancement techniques were also proposed in [Armero and Garikipati \(1996\)](#), [Simo et al. \(1993\)](#) and [Sluys \(1997\)](#) among others.

Discontinuous displacement fields were used to represent the strain jump across the band in the strong discontinuity approach, as in [Oliver \(1996\)](#), [Oliver et al. \(1999\)](#) and [Oliver and Huespe \(2004\)](#). To model shear bands using this technique, a specific strain softening material law was defined for the material inside the bands.

X-FEM techniques were used for modeling shear bands in [Samaniego and Belytschko \(2005\)](#) and [Areias and Belytschko \(2006\)](#) among other references. There the enhancement of the displacement field was performed with a fine scale strain function. A combination of X-FEM for the macroscale and FEM for the microscale was presented in [Belytschko et al. \(2007\)](#). This multiscale aggregating discontinuities method (MAD) excludes the subdomains with internal discontinuities from the coarser mesh and replaces them with an equivalent discontinuity to overcome instability using X-FEM. In the finer scale a unit cell is used to determine the behavior of the microscale under the loadings obtained from the larger scale. The multiple discontinuities existing in the microscale are aggregated into only one equivalent to be injected into the larger scale.

Our objective in the present paper is to extend the two-scale finite element formulation developed in [D'heres and Dvorkin \(2009\)](#) and [D'heres and Dvorkin \(2010\)](#) to model shear banding in G-T-N materials. For this purpose a stress localization criterion is also devised.

The paper is organized as follows: the G-T-N material formulation and the derivation of the stress localization criteria are presented in sections 2 and 3. The finite element formulation, the strong discontinuity modes and the virtual work principle are presented in sections 4, 5 and 6. The required interscales connection is attained via the equivalency of the dissipated work and the scales relation is derived for G-T-N material, in section 7. A test case is conducted in section 8 and the conclusions are stated in section 9.

## 2 THE G-T-N MATERIAL MODEL

The Gurson plasticity material model was first presented in Gurson (1975) and Gurson (1977) with the objective of modelling ductile porous media. Such materials show an increase in their void content during the plastic flow. Since the model introduction a number of modifications were proposed to adjust its parameters and a third void growth mechanism due to coalescence was added, see Tvergaard et al. (1981), Tvergaard (1981) and Tvergaard and Needleman (1984). The complete set is now called the Gurson-Tvergaard-Needleman material model.

The yield surface  ${}^t\Phi$  depends on the hydrostatic stress  ${}^t\sigma_h$ , the  $J_2$  equivalent stress  ${}^t\sigma_e$  and internal state variables,  ${}^t\zeta^i$  ( $i=1..$ number of internal state variables),

$${}^t\Phi({}^t\sigma_h, {}^t\sigma_e, {}^t\zeta^i) = 0, \quad (1)$$

$${}^t\sigma_h = \frac{1}{3} {}^t\underline{\underline{\sigma}} : {}^t\underline{\underline{\mathbf{g}}}, \quad (2)$$

$${}^t\sigma_e = \sqrt{\frac{3}{2} {}^t\underline{\underline{\sigma}} : {}^t\underline{\underline{\mathbf{s}}}}, \quad (3)$$

being  ${}^t\underline{\underline{\mathbf{s}}}$  the deviatoric stress tensor and  ${}^t\underline{\underline{\mathbf{g}}}$  the metric tensor.<sup>1</sup>

Explicitly the yield surface is defined in Tvergaard and Needleman (1984) as,

$${}^t\Phi = \left(\frac{{}^t\sigma_e}{{}^t\sigma_y}\right)^2 + 2 {}^t f q_1 \cosh({}^t\alpha) - 1 - {}^t f^2 q_1^2, \quad (4)$$

with,

$${}^t\alpha = \frac{3}{2} q_2 \frac{{}^t\sigma_h}{{}^t\sigma_y}. \quad (5)$$

The parameters  $q_1$  and  $q_2$  are set to fit the experimental results,  ${}^t f$  is the void volume fraction and  ${}^t\sigma_y$  is an equivalent tensile flow stress representing the actual microscopic stress-state. We adopt  $q_1 = 1.5$  and  $q_2 = 1$  for the present work, see Kopic and Needleman (1988).

The evolution of  ${}^t\sigma_y$  is modeled with an implicit hardening law presented in Aravas (1987),

$$\frac{{}^t\sigma_y}{{}^0\sigma_y} = \left(\frac{{}^t\sigma_y}{{}^0\sigma_y} + \frac{3 G}{{}^0\sigma_y} {}^t\bar{\varepsilon}^P\right)^N \quad (6)$$

where  ${}^0\sigma_y$  is the initial yield stress,  ${}^t\bar{\varepsilon}^P$  is the microscopic equivalent plastic strain and  $N$  is the hardening exponent. To determine  ${}^t\bar{\varepsilon}^P$ , it is assumed the equivalence of the microscopic and the macroscopic plastic work; hence,

$$(1 - {}^t f) {}^t\sigma_y d\bar{\varepsilon}^P = {}^t\underline{\underline{\sigma}} : d\underline{\underline{\varepsilon}}^P. \quad (7)$$

Then solving for  $d\bar{\varepsilon}^P$  we get,

$$d\bar{\varepsilon}^P = \frac{{}^t\underline{\underline{\sigma}} : d\underline{\underline{\varepsilon}}^P}{(1 - {}^t f) {}^t\sigma_y}. \quad (8)$$

We determine  ${}^t\sigma_e$  using the fact that during yielding  ${}^t\Phi = 0$  holds. Thus we solve for  ${}^t\sigma_e$  from Eqn. (4),

$${}^t\sigma_e^2 = {}^t\sigma_y^2 (1 + {}^t f^2 q_1^2 - 2 {}^t f q_1 \cosh({}^t\alpha)). \quad (9)$$

<sup>1</sup>We indicate the tensorial product between two tensors as  $\underline{\underline{a}} \underline{\underline{b}}$  and the number of underlines is the tensor order.

In the absence of distortive stresses, we can define the hydrostatic stress required to produce yielding. Hence using  ${}^t\sigma_e = 0$  in Eqn. (9) we get,

$${}^t\sigma_{hLimit} = \frac{2}{3q_2} {}^t\sigma_y \operatorname{arccosh} \left( \frac{1 + {}^t f^2 q_1^2}{2 {}^t f q_1} \right). \quad (10)$$

The void content growth is associated with three mechanisms:

- The growth of existing voids, driven by the bulk deformation,

$$df_{growth} = (1 - {}^t f) d\underline{\underline{\varepsilon}}^P : \underline{\underline{g}} \quad (11)$$

- The nucleation of new voids, driven by the plastic deformation,

$$df_{nucleation} = {}^t A d\bar{\varepsilon}^P \quad (12)$$

where  ${}^t A$  is a distribution function. We define function  ${}^t A$  based on the assumption that the void nucleation rate has a normal distribution as suggested in [Chu and Needleman \(1980\)](#),

$${}^t A = \frac{f_N}{s_N \sqrt{2\pi}} \exp \left[ -\frac{1}{2} \left( \frac{{}^t \bar{\varepsilon}^P - \varepsilon_N}{s_N} \right)^2 \right]. \quad (13)$$

In the above equation,  $f_N$  is the void volume fraction of nucleating particles,  $s_N$  its standard deviation and  $\varepsilon_N$  the mean strain for void nucleation. We adopt  $s_N = 0.1$ ,  $f_N = 0.04$  and  $\varepsilon_N = 0.3$ .

- The coalescence mechanism, driven by the void content. It is included into the yield condition by modifying  ${}^t f$  once a critical void fraction,  $f_{Crit}$ , is reached, see [Tvergaard and Needleman \(1984\)](#). Then, when the  $f_{Fract}$  value is reached, the material is assumed to loose all its load carrying capacity thus opening a crack. The values adopted are  $f_{Crit} = 0.15$  and  $f_{Fract} = 0.25$ . The pseudocode for this modification is as follows,

$${}^t f_{Mod} = \begin{cases} {}^t f & {}^t f < f_{Crit} \\ f_{Critical} + \frac{f_{Fract} - f_{Critical}}{f_{Fract} - f_{Crit}} ({}^t f - f_{Crit}) & f_{Crit} < {}^t f < f_{Fract} \end{cases} \quad (14)$$

$${}^t f = {}^t f_{Mod} \quad (15)$$

It must be noted that the internal variables that describe the deformation history are  ${}^t f$  and  ${}^t \bar{\varepsilon}^P$ , with explicit dependence of the yield surface (Eqn. (4)) on  ${}^t f$  and implicit on  ${}^t \bar{\varepsilon}^P$  through Eqns. (6) and (13).

The plastic strain increment results naturally split into volumetric and deviatoric contributions by chain derivation of the associated flow rule as is discussed in [Aravas \(1987\)](#),

$$d\underline{\underline{\varepsilon}}^P = d\lambda \frac{\partial {}^t \Phi}{\partial {}^t \underline{\underline{\sigma}}} = d\lambda \left( \frac{1}{3} \frac{\partial {}^t \Phi}{\partial {}^t \sigma_h} \underline{\underline{g}} + \frac{\partial {}^t \Phi}{\partial {}^t \sigma_e} \underline{\underline{\eta}} \right) \quad (16)$$

where  $\underline{\underline{\eta}}$  is the deviatoric direction tensor,

$$\underline{\underline{\eta}} = \frac{3}{2} \frac{\underline{\underline{g}}}{{}^t \sigma_e}. \quad (17)$$

The tensor  ${}^t\underline{\underline{\eta}}$  can be determined from the converged state or from the elastic trial state as the return to the yield surface is along it, Aravas (1987).

$${}^t\underline{\underline{\eta}} = \frac{3}{2} \frac{{}^t\underline{\underline{\mathbf{s}}}^E}{{}^t\sigma_e^E}. \tag{18}$$

being  ${}^t\underline{\underline{\mathbf{s}}}^E$  the trial elastic stress tensor.

The integration of the plastic strain (Eqn. (16)) using a backward Euler scheme, provides the increment of plastic strain from  $t$  to  $t + \Delta t$ ,

$$\underline{\underline{\epsilon}}^P = {}^{t+\Delta t}\underline{\underline{\epsilon}}^P - {}^t\underline{\underline{\epsilon}}^P = \frac{1}{3}\epsilon_h^P {}^{t+\Delta t}\underline{\underline{\mathbf{g}}} + \epsilon_e^P {}^{t+\Delta t}\underline{\underline{\eta}}, \tag{19}$$

where  $\epsilon_h^P$  is the volumetric plastic strain increment and  $\epsilon_e^P$  is the distortive plastic strain increment defined as,

$$\epsilon_h^P = \lambda \frac{\partial {}^t\Phi}{\partial {}^t\sigma_h} \tag{20}$$

$$\epsilon_e^P = \lambda \frac{\partial {}^t\Phi}{\partial {}^t\sigma_e}. \tag{21}$$

Eliminating  $\lambda$  from the previous we get,

$$\epsilon_h^P \frac{\partial {}^t\Phi}{\partial {}^t\sigma_e} - \epsilon_e^P \frac{\partial {}^t\Phi}{\partial {}^t\sigma_h} = 0 \tag{22}$$

To determine the equivalent plastic strain increment, we introduce Eqn. (19) into Eqn. (8) and integrate it backward Euler to get,

$$\bar{\epsilon}^P = {}^{t+\Delta t}\bar{\epsilon}^P - {}^t\bar{\epsilon}^P = \frac{{}^{t+\Delta t}\sigma_h \epsilon_h^P + {}^{t+\Delta t}\sigma_e \epsilon_e^P}{(1 - {}^{t+\Delta t}f) {}^{t+\Delta t}\sigma_y} \tag{23}$$

The void growth is found integrating the addition of Eqns. (11) and (12). Then considering Eqn. (19) we get the void volume fraction increment between  $t$  and  $t + \Delta t$

$${}^{t+\Delta t}f - {}^tf = f = (1 - {}^{t+\Delta t}f) \epsilon_h^P + {}^{t+\Delta t}A \bar{\epsilon}^P \tag{24}$$

Summarizing the calculation procedure, Eqns. (23) and (24) are the evolution of the internal variables, and have to be solved simultaneously with Eqns. (4) and (22) to determine the new state at  $t + \Delta t$ .

### 3 BIFURCATION DETECTION

We proceed with the determination of a stress based criterion for the bifurcation detection for the G-T-N material model based on the acoustic tensor properties. We state the fourth order constitutive tensor for the G-T-N material, see Sánchez et al. (2008) and Zhang and Niemi (1995),

$${}^t\underline{\underline{\mathbf{C}}}^{EP} = {}^t\underline{\underline{\mathbf{C}}}^E - \frac{\left( {}^t\underline{\underline{\mathbf{C}}}^E : {}^t\underline{\underline{\mathbf{M}}} \right) \left( {}^t\underline{\underline{\mathbf{M}}} : {}^t\underline{\underline{\mathbf{C}}}^E \right)}{t\xi ({}^tf, {}^t\bar{\epsilon}^P, {}^t\sigma_h)} \tag{25}$$

where  ${}^t\underline{\underline{\underline{\mathbf{C}}}}^{\mathbf{E}}$  is the elastic isotropic constitutive tensor  $\left({}^t\underline{\underline{\underline{\mathbf{C}}}}^{\mathbf{E}} = \frac{2\nu G}{1-2\nu} {}^t\underline{\underline{\mathbf{g}}} {}^t\underline{\underline{\mathbf{g}}} + 2G {}^t\underline{\underline{\mathbf{I}}}\right)$ ,  ${}^t\underline{\underline{\mathbf{M}}}$  is the plastic direction tensor  $\left({}^t\underline{\underline{\mathbf{M}}} = \frac{\partial {}^t\Phi}{\partial {}^t\underline{\underline{\boldsymbol{\sigma}}}}\right)$  and  ${}^t\xi$  is a positive scalar function dependent on  ${}^t\sigma_h$  and on the internal variables  ${}^tf$  and  ${}^t\bar{\varepsilon}^P$ .

The function  ${}^t\xi$  is,

$${}^t\xi({}^tf, {}^t\bar{\varepsilon}^P, {}^t\sigma_h) = \left({}^t\underline{\underline{\mathbf{M}}} : {}^t\underline{\underline{\underline{\mathbf{C}}}}^{\mathbf{E}} : {}^t\underline{\underline{\mathbf{M}}}\right) - {}^tN_\xi (1 - {}^tf) \text{trace}({}^t\underline{\underline{\mathbf{M}}}) \quad (26)$$

$$- ({}^tN_\xi {}^tA + {}^tR) \frac{{}^t\underline{\underline{\boldsymbol{\sigma}}} : {}^t\underline{\underline{\mathbf{M}}}}{(1 - {}^tf) {}^t\sigma_y}, \quad (27)$$

and,

$${}^t\xi({}^tf, {}^t\bar{\varepsilon}^P, {}^t\sigma_h) > 0.$$

In the previous Eqns. (25) and (26), the fact that Eqn. (9) holds and the following definitions and results adopted from Sánchez et al. (2008) have been used,

$${}^t\underline{\underline{\mathbf{M}}} = \frac{q_1 q_2}{{}^t\sigma_y} {}^tf \sinh({}^t\alpha) {}^t\underline{\underline{\mathbf{g}}} + \frac{3}{{}^t\sigma_y^2} {}^t\underline{\underline{\mathbf{s}}} \quad (28)$$

$${}^tN_\xi = (2 q_1 \cosh({}^t\alpha) - 2 q_1^2 {}^tf) {}^tH_f$$

$${}^tR = (4 q_1 {}^tf \cosh({}^t\alpha) - 2 - 2 q_1^2 {}^tf^2 - {}^t\sigma_h \text{trace}({}^t\underline{\underline{\mathbf{M}}})) \frac{{}^tH}{{}^t\sigma_y}$$

$${}^tH = \left. \frac{\partial \sigma_y}{\partial \bar{\varepsilon}^P} \right|_t$$

$${}^tH_f = \left. \frac{\partial f_{\text{Modified}}}{\partial f} \right|_t$$

To simplify the algebraic operations, we set a convenient Cartesian coordinate system  ${}^t\hat{\underline{\underline{\mathbf{x}}}}_i$  aligned to the band with  ${}^t\hat{\underline{\underline{\mathbf{x}}}}_1$  in the  ${}^t\underline{\underline{\mathbf{n}}}$ -direction and  ${}^t\hat{\underline{\underline{\mathbf{x}}}}_2$  in the  ${}^t\underline{\underline{\mathbf{m}}}$ -direction and build a  $D$  function as the determinant of the acoustic tensor,

$$D = \det \left( {}^t\hat{\underline{\underline{\mathbf{x}}}}_1 \cdot {}^t\underline{\underline{\underline{\mathbf{C}}}}^{\mathbf{EP}} \cdot {}^t\hat{\underline{\underline{\mathbf{x}}}}_1 \right) \quad (29)$$

The limit value for  ${}^t\sigma_e$  expressed in Eqn. (9) becomes a restriction because the stress state has to be on the yield surface in order to bifurcate, since no localization is possible inside the yield surface Ottosen and Runesson (1991).

We introduce the fact that stress deviator components are not mutually independent as Eqns. (3) and (9) hold, therefore we determine a suitable restriction for the deviatoric components  ${}^t\hat{s}_{12}$  and  ${}^t\hat{s}_{13}$ ,

$${}^t\hat{s}_{12}^2 + {}^t\hat{s}_{13}^2 = \frac{{}^t\sigma_y^2}{3} (1 + {}^tf^2 q_1^2 - 2 {}^tf q_1 \cosh({}^t\alpha)) - ({}^t\hat{s}_{11}^2 + {}^t\hat{s}_{22}^2 + {}^t\hat{s}_{11} {}^t\hat{s}_{22} + {}^t\hat{s}_{23}^2) \quad (30)$$

Replacing Eqns. (9) and (30) into (29) we get after some laborious algebra,

$$D_G = Q ({}^t\hat{s}_{11}^2 + Q_1 ({}^t\hat{s}_{22}^2 + {}^t\hat{s}_{11} {}^t\hat{s}_{22} + {}^t\hat{s}_{23}^2) - Q_2 - Q_3 {}^t\hat{s}_{11}) \quad (31)$$

where a set of constants that do not depend on the orientation of the coordinate system  ${}^t\hat{\mathbf{x}}_i$  have been defined,

$$Q = 36 \frac{G^4}{{}^t\sigma_y^4 {}^t\xi (1 - 2\nu)}$$

$$Q_1 = 2(1 - \nu)$$

$$Q_2 = {}^t\sigma_y^4 (1 - \nu) \left( \frac{{}^t\xi}{18G} - \frac{\left(\frac{1+\nu}{9}\right)^2 \text{trace}({}^t\mathbf{M})^2}{(1 - \nu)(1 - 2\nu)} + \frac{4 q_1 {}^t f \cosh({}^t\alpha) - 2 - 2(q_1 {}^t f)^2}{3 {}^t\sigma_y^2} \right)$$

$$Q_3 = \frac{2}{9} \text{trace}({}^t\mathbf{M}) {}^t\sigma_y^2 (1 + \nu)$$

To find a necessary condition for bifurcation, independently from stress deviator components, we assume a certain known internal variables state defined by  ${}^t f$  and  ${}^t\bar{\varepsilon}^P$  along with  ${}^t\sigma_h$  and then look for the extremum of  $D$  with respect to  ${}^t\hat{s}_{11}$ ,  ${}^t\hat{s}_{22}$  and  ${}^t\hat{s}_{23}$ . By differentiation it comes out that there is only one extremum located at,

$${}^t\hat{s}_{11} = \frac{2}{9} \text{trace}({}^t\mathbf{M}) {}^t\sigma_y^2 \quad (32)$$

$${}^t\hat{s}_{22} = -\frac{1}{9} \text{trace}({}^t\mathbf{M}) {}^t\sigma_y^2$$

$${}^t\hat{s}_{23} = 0$$

This extremum is a minimum since the *Hessian* of  $D$  is always positive definite.

Summarizing, as  $D$  is continuous and has only one extremum for any known state, if at this extremum  $D \leq 0$  it would imply that  $D$  vanishes at some region in the independent deviatoric stresses space  $({}^t\hat{s}_{11}, {}^t\hat{s}_{22}, {}^t\hat{s}_{23})$  or at least at a point. Therefore Eqn. (31) evaluated at the deviatoric stresses resulting from Eqns. (32),

$$\frac{1}{2} \frac{{}^t\xi}{G} + 6 \frac{2 q_1 {}^t f \cosh({}^t\alpha) - 1 - (q_1 {}^t f)^2}{{}^t\sigma_y^2} - \frac{(1 + \nu) \text{trace}({}^t\mathbf{M})^2}{3(1 - 2\nu)} \leq 0, \quad (33)$$

becomes a necessary condition for bifurcation in G-T-N materials. It is a necessary condition and not a sufficient one since the requirement for the stress state being able to satisfy conditions stated in Eqn. (32) simultaneously at  ${}^t\mathbf{n}$ -direction is too restrictive. This is due to the fact that a stress state could be able to fulfill  $D \leq 0$  at some point in the deviatoric stress space, nevertheless not being able to reach the absolute minimum of  $D$ .

Although Eqn. (33) is not a sufficient condition, it is useful for studying the parameters influence on localization. To focus on variables that trigger the localization, we adopt the following set of G-T-N material parameters:  $E = 200GPa$ ,  ${}^0\sigma_y = 600MPa$ , and  $\nu = 0.3$ . In Figs. 1 and 2 we map the region of the  ${}^t f - \left(\frac{{}^t\sigma_h}{{}^t\sigma_y}\right)$  (Relative hydrostatic stress) plane where the necessary condition is fulfilled for increasing levels of  ${}^t\bar{\varepsilon}^P$ ; on the same plane we plot  ${}^t\sigma_{hLimit}$ , see Sánchez et al. (2008). In Fig. 1 it can be seen that for a null hardening exponent  $N$ , the feasibility of bifurcation advances towards the compressive region when  ${}^t\bar{\varepsilon}^P$  is increased. As no hardening is present,  ${}^t\sigma_{hLimit}$  is the same for every  ${}^t\bar{\varepsilon}^P$ . It must be noted that for this situation with no voids present, the localization results are coincident with those obtained for  $J_2$  von Mises plasticity.

Increasing the hardening parameter to  $N = 0.1$ , in Fig. 2, the localization feasibility gets closer to  ${}^t\sigma_{hLimit}$  and the area of localization with null  ${}^t\bar{\varepsilon}^P$  vanishes following the previous tendency. In this figure the admissibility limits are clearly distinguishable due to the high hardening.

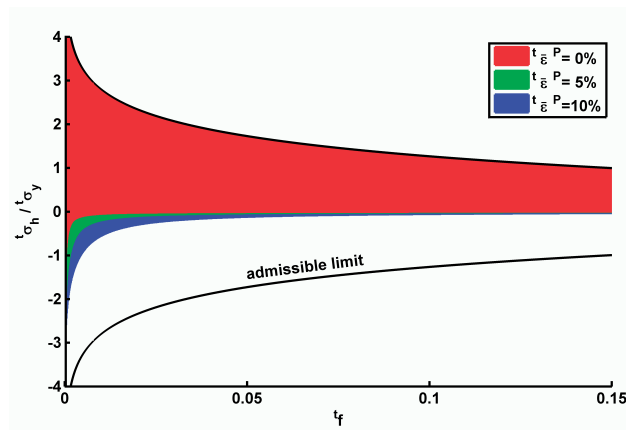


Figure 1: Necessary condition fulfillment with N=0.

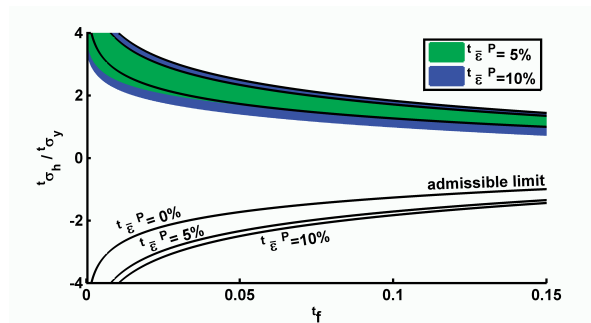


Figure 2: Necessary condition fulfillment with N=0.1.

To state the sufficient condition for localization, assuming Eqn. (33) is fulfilled, we must determine if the available stress deviatoric components can satisfy  $D \leq 0$  for some  $t_{\underline{n}}$  direction. For simplicity we restrict the following analysis to plane problems, but a three-dimensional problem could be solved adding the second projection angle. Thus we adopt  $t_{\hat{s}_{23}} = 0$  for plane strain.

To find the angle  $\beta$  where  $D$  is minimum we state the deviator stresses in the coordinate system  $\hat{x}_i$  referred to the global coordinates system  $x_i$ , and introduce them into (31). Thus we get,

$$D = R + R_1 \sin(2\beta) + R_2 \cos(2\beta) + R_3 \sin(4\beta) + R_4 \cos(4\beta) \tag{34}$$

with the following constants dependent on the actual stress state:

$$\begin{aligned}
 R &= ({}^t s_{11} + {}^t s_{22})^2 \left( \frac{5}{4} - \nu \right) + \frac{({}^t s_{11} - {}^t s_{22})^2}{8} - Q_3 \frac{({}^t s_{11} + {}^t s_{22})}{2} + {}^t s_{12}^2 + Q_2 \\
 R_1 &= {}^t s_{12} (Q_3 + ({}^t s_{11} + {}^t s_{22}) (1 - 2\nu)) \\
 R_2 &= \frac{({}^t s_{11} - {}^t s_{22})}{2} (Q_3 - ({}^t s_{11} + {}^t s_{22}) (1 - 2\nu)) \\
 R_3 &= -\frac{({}^t s_{11} - {}^t s_{22})}{2} {}^t s_{12} \\
 R_4 &= \frac{1}{2} \left( \frac{{}^t s_{11} - {}^t s_{22}}{2} \right)^2 - \frac{1}{2} {}^t s_{12}^2
 \end{aligned}$$

As no closed form for the minima of  $D$  could be found,  $\beta$  is determined via a global search in the interval  $(-\pi/2, \pi/2)$  and then a bisection algorithm is performed to improve the result. It must be noted that the  $N$  parameter has no influence in direction obtained from the the necessary condition fulfilment as deviatoric stresses in Eqn. (34) results scaled by  ${}^t \sigma_y$ .

The resulting condition depends on the stress deviator and the internal variables. To investigate its behavior we plot the angle between the localization and the maximum shear direction in the scaled deviatoric space  $\left( \frac{{}^t s_{11}}{{}^t \sigma_y} \right) - \left( \frac{{}^t s_{22}}{{}^t \sigma_y} \right)$  for several parameter sets. In addition scaled shear  $\left( \frac{{}^t s_{12}}{{}^t \sigma_y} \right)$  isolines are added to the plot for better understanding.

In Fig. 3 it can be seen that the localization angle coincides with the maximum shear for low  ${}^t f = 0.001, {}^t \bar{\epsilon}^P = 0.001$  and  ${}^t \sigma_h = 0.06MPa$ . In Fig. 4, increasing the parameters up to  ${}^t f = 0.1, {}^t \bar{\epsilon}^P = 0.1$  and  ${}^t \sigma_h = 600MPa$  the localization area moves towards positive  ${}^t s_{11}$ . In this case we find a significant difference between the maximum shear direction and the localization one. The contraction of the admissible stresses in all the figures is due to the  ${}^t f$  growth.

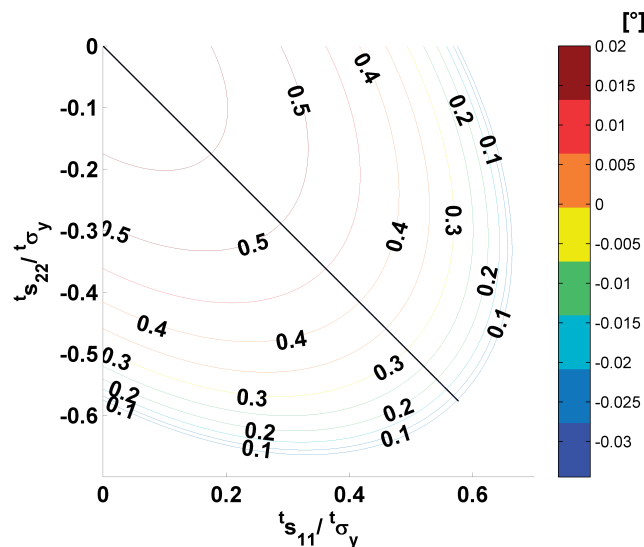


Figure 3: Angle between localization and maximum shear directions [°] for  ${}^t f = 0.001, {}^t \bar{\epsilon}^P = 0.001$ . and  ${}^t \sigma_h = 0.06MPa$ .

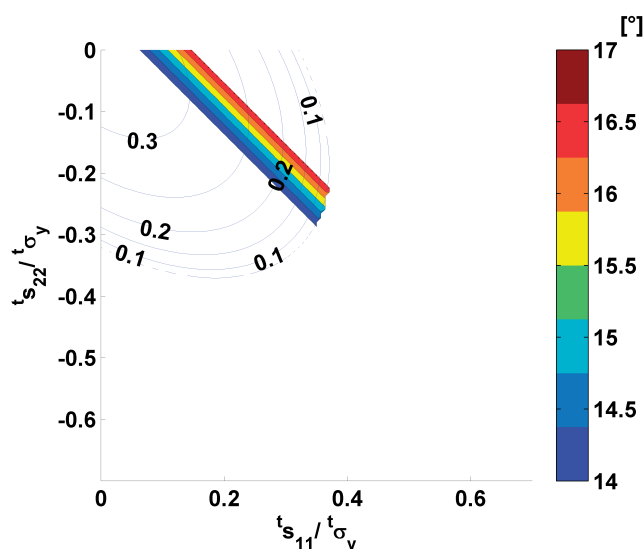


Figure 4: Angle between localization and maximum shear directions [°] for  ${}^t f = 0.1$ ,  ${}^t \bar{\varepsilon}^P = 0.1$  and  ${}^t \sigma_h = 600 \text{MPa}$ .

Summarizing, the resulting procedure for localization detection is as follows: if Eqn. (33) is fulfilled we find the  $\beta$  angle that minimizes Eqn. (34). If there  $D \leq 0$  then the material localizes at  $\beta$  direction, if not the bifurcation is precluded.

#### 4 FINITE ELEMENT FORMULATION

We solve the nonlinear problems using an incremental procedure. Hence we write,

$${}^{t+\Delta t} \underline{u} = {}^t \underline{u} + \underline{u}. \quad (35)$$

where,  ${}^{t+\Delta t} \underline{u}$  : is the displacement field at  $(t + \Delta t)$ -configuration,  ${}^t \underline{u}$  is the displacement field that defines the  $(t)$ -configuration and  $\underline{u}$  is the incremental displacement field that goes from the  $(t)$ -configuration to the  $(t + \Delta t)$ -configuration.

We discretize the continuum using the finite element method, see Bathe (1996.), interpolating in every element the displacement field using interpolation matrix  $\underline{\mathbf{H}}(x, y, z)$  and the respective nodal displacements vectors  ${}^{t+\Delta t} \underline{\mathbf{U}}$ ,  ${}^t \underline{\mathbf{U}}$  and  $\underline{\mathbf{U}}$ ,

$${}^{t+\Delta t} \underline{u} = \underline{\mathbf{H}} {}^{t+\Delta t} \underline{\mathbf{U}} = \underline{\mathbf{H}} {}^t \underline{\mathbf{U}} + \underline{\mathbf{H}} \underline{\mathbf{U}}. \quad (36)$$

To be able to describe the continuum displacement and the localization mechanism, the incremental displacement field is decomposed into continuum and localized contributions:

$$\underline{u} = \underline{u}_{cont} + \underline{u}_{loc}. \quad (37)$$

These contributions are also interpolated using the interpolation matrix  $\underline{\mathbf{H}}$  and the respective incremental nodal displacements  $\underline{\mathbf{U}}_{cont}$  and  $\underline{\mathbf{U}}_{loc}$ . Hence it results that the total increment of nodal displacements is,

$$\underline{\mathbf{U}} = \underline{\mathbf{U}}_{cont} + \underline{\mathbf{U}}_{loc}. \quad (38)$$

To model the localization mechanism, we introduce a specific deformation mode  $\underline{\Theta}$  into the formulation,

$$\underline{\mathbf{U}}_{loc} = \gamma \underline{\Theta}, \quad (39)$$

where  $\gamma$  is the increment of a scalar parameter that is used to determine the localization mechanism evolution. The incremental relation for the parameter  $\gamma$  is,

$${}^{t+\Delta t}\gamma = {}^t\gamma + \gamma. \quad (40)$$

Therefore evaluating Eqn. (37) we get,

$$\underline{u} = \underline{\mathbf{H}} \underline{\mathbf{U}} = \underline{\mathbf{H}} (\underline{\mathbf{U}} - \gamma \underline{\Theta}) + \underline{\mathbf{H}} \gamma \underline{\Theta} \quad (41)$$

where we recognize that,

$$\underline{u}_{cont} = \underline{\mathbf{H}} (\underline{\mathbf{U}} - \gamma \underline{\Theta}) \quad (42)$$

$$\underline{u}_{loc} = \underline{\mathbf{H}} \gamma \underline{\Theta}. \quad (43)$$

Here it must be noted that  $\underline{u}_{cont}$  represents the displacement in the continuum and  $\underline{u}_{loc}$  represents the displacement induced by the localization and both are distributed along the element domain. The continuum contribution is physically meaningful since it is defined in the proper scale, but the localized contribution does not, since it distributes the localization effect over the element domain.

## 5 MODE CONSTRUCTION

The construction of the  $\underline{\Theta}$  modes was presented for  $J_2$  materials in D'heres and Dvorkin (2009) and D'heres and Dvorkin (2010), where it is considered that the localization mechanism behaves as rigid-plastic, neglecting therefore its elastic component. For the strain field we also use an additive decomposition; considering infinitesimal strains we get,

$${}^{t+\Delta t}\underline{\underline{\varepsilon}} = {}^t\underline{\underline{\varepsilon}} + \underline{\underline{\varepsilon}}. \quad (44)$$

The deformation increment  $\underline{\underline{\varepsilon}}$  is decomposed into elastic and plastic parts and the elastic strain increment only contributes to the continuum scale but the plastic deformation increment contributes to the continuum and to the localized scales,

$$\underline{\underline{\varepsilon}} = \underline{\underline{\varepsilon}}_{cont}^E + \underline{\underline{\varepsilon}}_{cont}^P + \underline{\underline{\varepsilon}}_{loc}^P. \quad (45)$$

Using the Eqns. (42) and (43) we get,

$$\underline{\underline{\varepsilon}}_{cont} = \underline{\underline{\varepsilon}}_{cont}^E + \underline{\underline{\varepsilon}}_{cont}^P = \underline{\mathbf{B}} (\underline{\mathbf{U}} - \gamma \underline{\Theta}) \quad (46)$$

$$\underline{\underline{\varepsilon}}_{loc} = \underline{\underline{\varepsilon}}_{loc}^P = \underline{\mathbf{B}} \underline{\mathbf{U}}_{loc} = \underline{\mathbf{B}} \gamma \underline{\Theta}, \quad (47)$$

where  $\underline{\mathbf{B}}$  is the element strain-displacement matrix and the  $\underline{\underline{\varepsilon}}_{cont}^E$ ,  $\underline{\underline{\varepsilon}}_{cont}^P$  and  $\underline{\underline{\varepsilon}}_{loc}^P$  are the respective strain tensor components arrays resulting from adoption of the Voigt notation<sup>2</sup>.

To construct the  $\underline{\Theta}$  mode we impose two conditions on it:

<sup>2</sup>The strain components in the xy plane for plane problems are:

- for plane stress cases  $\underline{\underline{\varepsilon}}^T = [ \varepsilon_1 \quad \varepsilon_2 \quad \varepsilon_4 ] = [ \varepsilon_{xx} \quad \varepsilon_{yy} \quad 2\varepsilon_{xy} ]$ ,
- for plane strain and axisymmetric cases  $\underline{\underline{\varepsilon}}^T = [ \varepsilon_1 \quad \varepsilon_2 \quad \varepsilon_3 \quad \varepsilon_4 ] = [ \varepsilon_{xx} \quad \varepsilon_{yy} \quad \varepsilon_{zz} \quad 2\varepsilon_{xy} ]$

- It has to have its maximum distortional deformation aligned with the band (defined by angle  $\beta$ , which is the angle between directions  ${}^t\mathbf{n}$  and  ${}^t\mathbf{x}_1$ )

$$\frac{\varepsilon_{loc4}}{\varepsilon_{loc1} - \varepsilon_{loc2}} = \tan\left(2\beta + \frac{\pi}{2}\right) \quad (48)$$

- The volume strain has to be controlled,

$$\varepsilon_{loc1} + \varepsilon_{loc2} + \varepsilon_{loc3} = \varepsilon_{locv}. \quad (49)$$

To build  $\underline{\Theta}$  for the particular case of 2D elements, we recall that a 4 – node quadrilateral element formulated in the isoparametric natural element space  $(r, s)$  has  $2N$  eigenmodes among which there can be found: two pure shear modes, one with its maximum distortion tilted from the axes by  $\frac{\pi}{4}$  and one with the maximum distortion aligned with the axes, and one volume change mode. By linearly combining these modes we can construct a *shear base* so as to obtain a pure shear mode in any desired direction and add a volume change mode to control the volumetric strainig.

We compute the strain components at the element center from the three modes,

$$\begin{aligned} \underline{\varepsilon}_I &= \underline{\mathbf{B}}_c \underline{\Psi}_I \\ \underline{\varepsilon}_{II} &= \underline{\mathbf{B}}_c \underline{\Psi}_{II} \\ \underline{\varepsilon}_{III} &= \underline{\mathbf{B}}_c \underline{\Psi}_{III} \end{aligned} \quad (50)$$

where  $\underline{\mathbf{B}}_c = \underline{\mathbf{B}}(x_1^o, x_2^o)$  is the strain-displacements matrix evaluated at the element center. The linear combination of the above defined strain fields results in the localization strains  $\underline{\varepsilon}_{loc}$ , where  $c_I$ ,  $c_{II}$  and  $c_{III}$  are constant parameters to be determined,

$$\underline{\varepsilon}_{loc} = c_I \underline{\varepsilon}_I + c_{II} \underline{\varepsilon}_{II} + c_{III} \underline{\varepsilon}_{III} = \underline{\mathbf{B}}_c (c_I \underline{\Psi}_I + c_{II} \underline{\Psi}_{II} + c_{III} \underline{\Psi}_{III}) \quad (51)$$

The G-T-N plastic evolution in a shear band does have volumetric strain besides distortive strain (Eqn. (23)). To include both effects in the  $\underline{\Theta}$  mode formulation, we decompose the band strain into two contributions: one distortive ( $\underline{\varepsilon}_{distortive}$ ) and one volumetric ( $\underline{\varepsilon}_{volumetric}$ ). For each of these contributions a strong discontinuity mode is obtained, a distortive mode ( $\underline{\Theta}_e$ ) and a volume change ( $\underline{\Theta}_h$ ) one.

The localization modes are determined linearly combining the strains belonging to the *shear base* (Eqns. (50)). Hence,

$$\underline{\varepsilon}_{distortive} = c_I^d \underline{\varepsilon}_I + c_{II}^d \underline{\varepsilon}_{II} + c_{III}^d \underline{\varepsilon}_{III} = \underline{\mathbf{B}}_c (c_I^d \underline{\Psi}_I + c_{II}^d \underline{\Psi}_{II} + c_{III}^d \underline{\Psi}_{III}) \quad (52a)$$

$$\underline{\varepsilon}_{volumetric} = c_I^v \underline{\varepsilon}_I + c_{II}^v \underline{\varepsilon}_{II} + c_{III}^v \underline{\varepsilon}_{III} = \underline{\mathbf{B}}_c (c_I^v \underline{\Psi}_I + c_{II}^v \underline{\Psi}_{II} + c_{III}^v \underline{\Psi}_{III}) \quad (52b)$$

where  $c_A^d$  and  $c_A^v$ , are two sets of constants. Both sets are determined independently using the conditions in Eqns.(48) and (49).

Hence we request for the  $\underline{\Theta}_e$  mode that  $\underline{\varepsilon}_{distortive}$  has its maximum distortional deformations aligned to the band angle  $\beta$  and no volume change. Thus,

$$\begin{aligned} \frac{\varepsilon_{distortive4}}{\varepsilon_{distortive1} - \varepsilon_{distortive2}} &= \tan\left(2\beta + \frac{\pi}{2}\right) \\ \varepsilon_{distortive1} + \varepsilon_{distortive2} + \varepsilon_{distortive3} &= 0, \end{aligned}$$

from where we determine  $c_I^d$ ,  $c_{II}^d$  and  $c_{III}^d$  imposing that  $c_{III}^d = 0$  if  $\underline{\epsilon}_I$  and  $\underline{\epsilon}_{II}$  are incompressible or  $c_{III}^d = 1$  otherwise.

Then, for the mode  $\underline{\Theta}_h$ , we request  $\underline{\epsilon}_{volumetric}$  to have only volume change and no distortion in any direction. Thus,

$$\begin{aligned} \epsilon_{volumetric_1} + \epsilon_{volumetric_2} + \epsilon_{volumetric_3} &= 1 \\ \epsilon_{volumetric_4} &= 0 \\ \epsilon_{volumetric_1} - \epsilon_{volumetric_2} &= 0 \end{aligned}$$

from where we determine  $c_I^v$ ,  $c_{II}^v$  and  $c_{III}^v$  imposing again that  $c_{III}^v = 0$  if  $\underline{\epsilon}_I$  and  $\underline{\epsilon}_{II}$  are incompressible or  $c_{III}^v = 1$  otherwise.

Finally we get the normalized modes,

$$\underline{\Theta}_e = \frac{c_I^d \underline{\Psi}_I + c_{II}^d \underline{\Psi}_{II} + c_{III}^d \underline{\Psi}_{III}}{|c_I^d \underline{\Psi}_I + c_{II}^d \underline{\Psi}_{II} + c_{III}^d \underline{\Psi}_{III}|} \tag{53}$$

$$\underline{\Theta}_h = \frac{c_I^v \underline{\Psi}_I + c_{II}^v \underline{\Psi}_{II} + c_{III}^v \underline{\Psi}_{III}}{|c_I^v \underline{\Psi}_I + c_{II}^v \underline{\Psi}_{II} + c_{III}^v \underline{\Psi}_{III}|}, \tag{54}$$

and their respective strains per unit  $\gamma$ ,

$$\begin{aligned} \check{\underline{\epsilon}}_{distortive} &= \underline{\mathbf{B}}_c \underline{\Theta}_e \\ \check{\underline{\epsilon}}_{volumetric} &= \underline{\mathbf{B}}_c \underline{\Theta}_h. \end{aligned} \tag{55}$$

Now we get the localization strains per unit  $\gamma$ ,  $\check{\underline{\epsilon}}_{loc}$ , combining the strain contributions scaled by parameters  $a_e$  and  $a_h$ ,

$$\check{\underline{\epsilon}}_{loc} = a_e \check{\underline{\epsilon}}_{distortive} + a_h \check{\underline{\epsilon}}_{volumetric}, \tag{56}$$

where the strains  $\check{\underline{\epsilon}}_{loc}$ ,  $\check{\underline{\epsilon}}_{distortive}$  and  $\check{\underline{\epsilon}}_{volumetric}$  are written in tensor form instead of a vector array.

To determine  $a_e$  and  $a_h$ , we resort to the continuum strains without localization present, i.e. the resulting strain if band is inactive. Therefore we enforce  $\check{\underline{\epsilon}}_{loc}$  to have the same proportion of volumetric and distortive strains as the continuum would have if the element band was closed. Equating Eqn. (19) to (56) we get,

$$\frac{1}{3} \epsilon_{continuum_h}^P \underline{\underline{\mathbf{g}}}^{t+\Delta t} + \epsilon_{continuum_e}^P \underline{\underline{\mathbf{\eta}}}^{t+\Delta t} = a_e \check{\underline{\epsilon}}_{distortive} + a_h \check{\underline{\epsilon}}_{volumetric} \tag{57}$$

To determine  $a_h$  and  $a_e$ , we project Eqn. (57) it onto  $\underline{\underline{\mathbf{g}}}^{t+\Delta t}$  and  $\underline{\underline{\mathbf{\eta}}}^{t+\Delta t}$  successively to get,

$$a_h = \frac{\epsilon_{continuum_h}^P}{\check{\underline{\epsilon}}_{volumetric} : \underline{\underline{\mathbf{g}}}^{t+\Delta t}} \tag{58}$$

$$a_e = \frac{3}{2} \frac{\epsilon_{continuum_e}^P}{\check{\underline{\epsilon}}_{distortive} : \underline{\underline{\mathbf{\eta}}}^{t+\Delta t}}. \tag{59}$$

We finally get the strong discontinuity mode combining modes  $\underline{\Theta}_e$  and  $\underline{\Theta}_h$  weighted by parameters  $a_h$  and  $a_e$  as in Eqn. (57),

$$\underline{\mathbf{B}}_c \underline{\Theta} = a_e \underline{\mathbf{B}}_c \underline{\Theta}_e + a_h \underline{\mathbf{B}}_c \underline{\Theta}_h. \tag{60}$$

At last we normalize the mode  $\underline{\Theta}$ ,

$$\underline{\Theta} = \frac{a_h \underline{\Theta}_h + a_e \underline{\Theta}_e}{|a_h \underline{\Theta}_h + a_e \underline{\Theta}_e|}$$

## 6 VIRTUAL WORK PRINCIPLE

To state the virtual work principle, we analyze a continuum subject to external forces crossed by a localization line, as shown in Fig. 5.

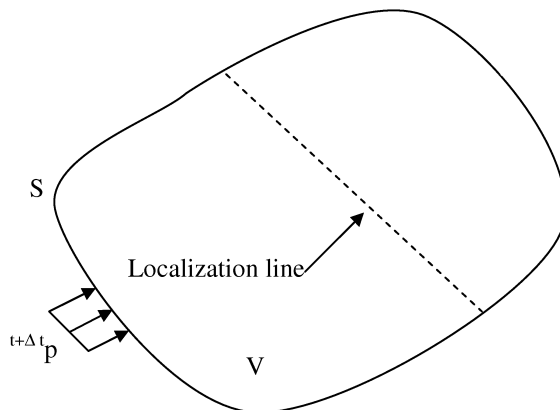


Figure 5: Continuum with a localized shear band

To determine the new configuration we use the virtual work principle for a “material nonlinear only analysis” (geometrically linear analysis) [Bathe \(1996\)](#). For this we need to determine the internal work in the volume  $V$ , the external forces work on the surface  $S$  and the band forces work  ${}^{t+\Delta t}\underline{\mathbf{F}}_{loc}$ . Equating the internal work and the band work to the external work equation we get the virtual work principle,

$$\int_V \delta \underline{\boldsymbol{\varepsilon}}_{cont}^T {}^{t+\Delta t} \underline{\boldsymbol{\sigma}}_{cont} dv + \delta \underline{\mathbf{U}}_{loc}^T {}^{t+\Delta t} \underline{\mathbf{F}}_{loc} = \int_S \delta \underline{\mathbf{u}}^T {}^{t+\Delta t} \underline{\mathbf{p}} ds. \quad (61)$$

The variations are determined using Eqns. (39), (46) and (41). Hence we get,

$$\delta \underline{\mathbf{U}}_{loc}^T = \delta \gamma \underline{\boldsymbol{\Theta}}^T, \quad (62)$$

$$\delta \underline{\boldsymbol{\varepsilon}}_{cont}^T = (\delta \underline{\mathbf{U}}^T - \delta \gamma \underline{\boldsymbol{\Theta}}^T) \underline{\mathbf{B}}^T \quad (63)$$

and,

$$\delta \underline{\mathbf{u}}^T = \delta \underline{\mathbf{U}}^T \underline{\mathbf{H}}. \quad (64)$$

For the continuum stresses we use the constitutive relation and Eqn. (46) to get,

$${}^{t+\Delta t} \underline{\boldsymbol{\sigma}}_{cont} = {}^t \underline{\boldsymbol{\sigma}}_{cont} + {}^t \underline{\mathbf{C}}^{EP} \underline{\boldsymbol{\varepsilon}}_{cont} = {}^t \underline{\boldsymbol{\sigma}}_{cont} + {}^t \underline{\mathbf{C}}^{EP} \underline{\mathbf{B}} (\underline{\mathbf{U}} - \gamma \underline{\boldsymbol{\Theta}}). \quad (65)$$

Replacing Eqns. (62), (63), (64) and (65) in Eqn. (61) and solving for  $\delta \underline{\mathbf{U}}$  and  $\delta \gamma$  and making use of the fact that  $\delta \underline{\mathbf{U}}$  and  $\delta \gamma$  are arbitrary we get,

$$\begin{bmatrix} {}^t \underline{\mathbf{K}}_u & -{}^t \underline{\mathbf{K}}_u \underline{\boldsymbol{\Theta}} \\ -\underline{\boldsymbol{\Theta}}^T {}^t \underline{\mathbf{K}}_u & \underline{\boldsymbol{\Theta}}^T {}^t \underline{\mathbf{K}}_u \underline{\boldsymbol{\Theta}} \end{bmatrix} \begin{bmatrix} \underline{\mathbf{U}} \\ \gamma \end{bmatrix} = \begin{bmatrix} {}^{t+\Delta t} \underline{\mathbf{R}} - {}^t \underline{\mathbf{F}} \\ \underline{\boldsymbol{\Theta}}^T ({}^t \underline{\mathbf{F}} - {}^{t+\Delta t} \underline{\mathbf{F}}_{loc}) \end{bmatrix}, \quad (66)$$

where we used,

$$\begin{aligned} {}^t\mathbf{K}_u &= \int_V \mathbf{B}^T {}^t\mathbf{C}^{EP} \mathbf{B} \, dv \\ {}^{t+\Delta t}\mathbf{R} &= \int_S \mathbf{H}^T {}^{t+\Delta t}\mathbf{p} \, ds \\ {}^t\mathbf{F} &= \int_V \mathbf{B}^T {}^t\boldsymbol{\sigma} \, dv. \end{aligned}$$

The resulting Eqns. (66) are non-linear and have to be solved iteratively.

## 7 LENGTH SCALE ADOPTION FOR G-T-N MATERIAL

In the equations system stated in Eqns. (66), all variables are readily known except  ${}^{t+\Delta t}\mathbf{F}_{loc}$ . Since during the deformation process the material remains inside the plastic range, its yield stress has to evolve as (D’hers and Dvorkin (2009)),

$${}^{t+\Delta t}\sigma_{yloc} = k {}^t\sigma_{yloc}. \tag{67}$$

and it can be assumed that the equivalent localized nodal forces have to also evolve radially; hence,

$$\mathbf{\Theta}^T {}^{t+\Delta t}\mathbf{F}_{loc} = k \mathbf{\Theta}^T {}^t\mathbf{F}_{loc}. \tag{68}$$

Solving for k in Eqns. (67) and (68) we determine the evolution of the band forces,

$$\mathbf{\Theta}^T {}^{t+\Delta t}\mathbf{F}_{loc} = \mathbf{\Theta}^T {}^t\mathbf{F}_{loc} \frac{{}^{t+\Delta t}\sigma_{yloc}}{{}^t\sigma_{yloc}}. \tag{69}$$

At the band direction the equilibrium is satisfied by Eqn. (69) where the material parameters belonging to the localized scale are inserted in the equation through  ${}^{t+\Delta t}\sigma_{yloc}$ , which is the inter-scales connecting variable.

If the shear band opens at the  $\tau$ -configuration, we have as initial condition for Eqn.(69),

$$\mathbf{\Theta}^T \tau \mathbf{F}_{loc} = \mathbf{\Theta}^T \tau \mathbf{F} = \mathbf{\Theta}^T \int_V \mathbf{B}^T \tau \boldsymbol{\sigma} \, dv.$$

Even though we are not intending to describe the micromechanical behavior inside the shear bands, we know that the phenomena that take place there is beyond the continuum mechanics hypothesis, since the band dimensions are in the granular size scale. For this reason, to model the band formation, we heuristically define a bandwidth to represent the above mentioned micro-scale evolution. The definition of this bandwidth allows the experimental calibration of the model and provides mesh independent results also insensitive to mesh distortions.

The determination of the yield stress required in Eqn. (69) in the G-T-N material differs from the  $J_2$  case because, the yield surface depends on  ${}^t\sigma_{hloc}$ ,  ${}^t f_{loc}$  and  ${}^t \bar{\epsilon}_{loc}^P$  parameters. Thus we define a modified yield stress,  ${}^t \bar{\sigma}_{yloc}$ , by means of Eqn. (9),

$${}^t \bar{\sigma}_{yloc} ({}^t f_{loc}, {}^t \sigma_{yloc}, {}^t \sigma_h) = {}^t \sigma_{yloc} \sqrt{\left(1 + {}^t f_{loc}^2 q_1^2 - 2 {}^t f_{loc} q_1 \cosh\left(\frac{3}{2} q_2 \frac{{}^t \sigma_{hloc}}{{}^t \sigma_{yloc}}\right)\right)}.$$

Its calculation requires the evaluation of the internal variables of the band. Hence, to model their evolution, we observe that the plastic deformation depends on the volumetric strain increment ( $\epsilon_{hloc}^P$ ) and the respective distortive equivalent strain ( $\epsilon_{e_{loc}}^P$ ), as shown in Eqn. (19).

These two strains are calculated in the band scale using two separate inter-scales factors,

$$(\varepsilon_{h_{loc}}^P)^2 = \zeta^2 \gamma^2, \quad (70)$$

$$(\varepsilon_{e_{loc}}^P)^2 = \varphi^2 \gamma^2. \quad (71)$$

To determine the inter-scales factors we recall that the localization mode  $\underline{\Theta}$  is built using two modes,  $\underline{\Theta}_e$  and  $\underline{\Theta}_h$ . We request the distortive dissipated energy in the band to be equal to the energy dissipated by the distortive part of the localization mode, and apply the same reasoning to relate the hydrostatic parts.

To derive these conditions, we use Eqn. (19) and the fact that the tensor  ${}^{t+\Delta t} \underline{\underline{\sigma}}_{loc}$  can be written as,

$${}^{t+\Delta t} \underline{\underline{\sigma}}_{loc} = {}^{t+\Delta t} \sigma_{h_{loc}} {}^{t+\Delta t} \underline{\underline{g}} + \frac{2}{3} {}^{t+\Delta t} \sigma_{e_{loc}} {}^{t+\Delta t} \underline{\underline{\eta}},$$

to get the band dissipated energy,

$$\int_{V_{loc}} \int_t^{t+\Delta t} {}^t \underline{\underline{\sigma}} : d\underline{\underline{\varepsilon}}^P dV_{loc} = \int_{V_{loc}} \left( \int_t^{t+\Delta t} {}^{t+\Delta t} \sigma_h d\varepsilon_{h_{loc}}^P + \int_t^{t+\Delta t} {}^{t+\Delta t} \sigma_e d\varepsilon_{e_{loc}}^P \right) dV_{loc} \quad (72)$$

There we clearly identify the distortive and the hydrostatic contributions to the energy dissipation. These contributions are equated to the respective mode energies to get,

$$\int_{t\gamma}^{t+\Delta t\gamma} \underline{\Theta}_e^T {}^{t+\Delta t} \underline{\underline{F}} d\gamma = \int_{V_{loc}} \int_t^{t+\Delta t} {}^{t+\Delta t} \sigma_e d\varepsilon_{e_{loc}}^P dV_{loc}, \quad (73)$$

and,

$$\int_{t\gamma}^{t+\Delta t\gamma} \underline{\Theta}_h^T {}^{t+\Delta t} \underline{\underline{F}} d\gamma = \int_{V_{loc}} \int_t^{t+\Delta t} {}^{t+\Delta t} \sigma_h d\varepsilon_{h_{loc}}^P dV_{loc}. \quad (74)$$

Assuming unitary thickness, the volume of material comprised in the localization is,

$$V_{loc} = h L, \quad (75)$$

where  $h$  is a reference bandwidth and  $L$  is the band length across the element.

Eqns. (73) and (74) are integrated Backward Euler using (75), to give,

$$\gamma \underline{\Theta}_e^T {}^{t+\Delta t} \underline{\underline{F}} = {}^{t+\Delta t} \sigma_e \varepsilon_{e_{loc}}^P h L, \quad (76)$$

and

$$\gamma \underline{\Theta}_h^T {}^{t+\Delta t} \underline{\underline{F}} = {}^{t+\Delta t} \sigma_h \varepsilon_{h_{loc}}^P h L. \quad (77)$$

Replacing  $\varepsilon_{e_{loc}}^P$  and  $\varepsilon_{h_{loc}}^P$  definitions into the previous we get the inter-scales factors,

$$\varphi = \left| \frac{\underline{\Theta}_e^T {}^{t+\Delta t} \underline{\underline{F}}_{loc}}{h L {}^{t+\Delta t} \sigma_{e_{loc}}} \right|,$$

$$\zeta = \left| \frac{\underline{\Theta}_h^T {}^{t+\Delta t} \underline{\underline{F}}}{h L {}^{t+\Delta t} \sigma_{h_{loc}}} \right|.$$

Now that a proper scale is defined for the band strains, we determine  $\varepsilon_{h_{loc}}^P$  and  $\varepsilon_{e_{loc}}^P$  from Eqns. (70) and (71). Finally we determine the internal variables increments using Eqns. (6), (13), (23) and (24) as,

$$\begin{aligned} \frac{{}^{t+\Delta t}\sigma_{y_{loc}}}{{}^0\sigma_y} &= \left( \frac{{}^{t+\Delta t}\sigma_{y_{loc}}}{{}^0\sigma_y} + \frac{3G}{{}^0\sigma_y} {}^{t+\Delta t}\bar{\varepsilon}_{loc}^P \right)^N, \\ {}^{t+\Delta t}A_{loc} &= \frac{f_N}{s_N\sqrt{2\pi}} \exp \left[ -\frac{1}{2} \left( \frac{{}^{t+\Delta t}\bar{\varepsilon}_{loc}^P - \varepsilon_N}{s_N} \right)^2 \right], \\ \bar{\varepsilon}_{loc}^P &= \frac{{}^{t+\Delta t}\sigma_{h_{loc}} \varepsilon_{h_{loc}}^P + {}^{t+\Delta t}\sigma_{e_{loc}} \varepsilon_{e_{loc}}^P}{(1 - {}^{t+\Delta t}f_{loc}) {}^{t+\Delta t}\sigma_{y_{loc}}}, \end{aligned}$$

and

$$f_{loc} = (1 - {}^{t+\Delta t}f_{loc}) \varepsilon_{h_{loc}}^P + {}^{t+\Delta t}A_{loc} ({}^{t+\Delta t}\bar{\varepsilon}_{loc}^P) \bar{\varepsilon}_{loc}^P.$$

The determination of the continuum scale evolution is carried out at the standard Gauss points. Aside from that, to detect the triggering of localization, we also determine the plastic evolution at the element center. When at that point the localization conditions are met during a step iteration process, as in Ortiz et al. (1987), the band displacement mode is added to the element, i.e. localization is activated. From then on the element center is used to describe the band scale, see D'heres and Dvorkin (2010).

## 8 TEST CASE

The criterion to open a band and the stabilization procedures required to achieve convergence are adopted from D'heres and Dvorkin (2010). The band triggering criterion is divided into three levels of decision to improve performance. First it is required that an increment in plasticity exists at the element center. Then in such case, the localization necessary condition is tested, and at last if it is true then the sufficient condition is used. The election between two alternative directions is necessary since the solution to Eqn. (34) does not have only one solution for the band angle,  $\beta$ . Following Samaniego and Belytschko (2005), for the first shear band that is triggered in the model we select one of the two directions and for the other ones we use a "persistence criterion", which means that in any new band opening we choose from the two possible directions, the one closer to the localization direction in the surrounding elements.

The solution of finer meshes showed that sometimes, after some band development has occurred, there are steps in which all the active bands achieve convergence except for one. We observe that the  $\gamma$ -value of the problematic element oscillates around a value near the convergence tolerance. We resorted to closing the band of the oscillating element during the step, as in D'heres and Dvorkin (2010). We find that this decision in most cases help convergence. Since this is an arbitrary decision, we investigated its impact and concluded that it has no measurable influence on the overall response and that the modified element does not require to be modified again in the following steps. Also we observed that the elements that required this stabilization were most of the times on the band borders.

The test case is a sheet with two symmetry planes and a central square notch to induce the localization (Fig. 6). We use the QMITC element (Dvorkin and Vassolo (1989)) with the localization mechanism included in its formulation. The use of a notch makes the defect weakening effect constant regardless the mesh refinement. We use as indicators, the behavior of the energy dissipated at the continuum scale, which is expected to decrease when the mesh

is refined, and the behavior of the energy dissipated at the shear band scale, which is expected to converge when the mesh is refined.

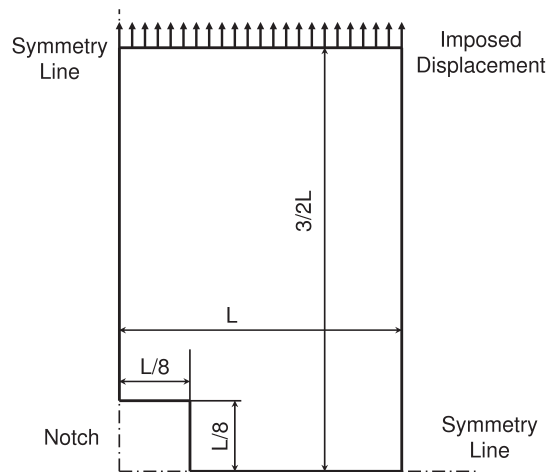


Figure 6: Notched sample for traction test

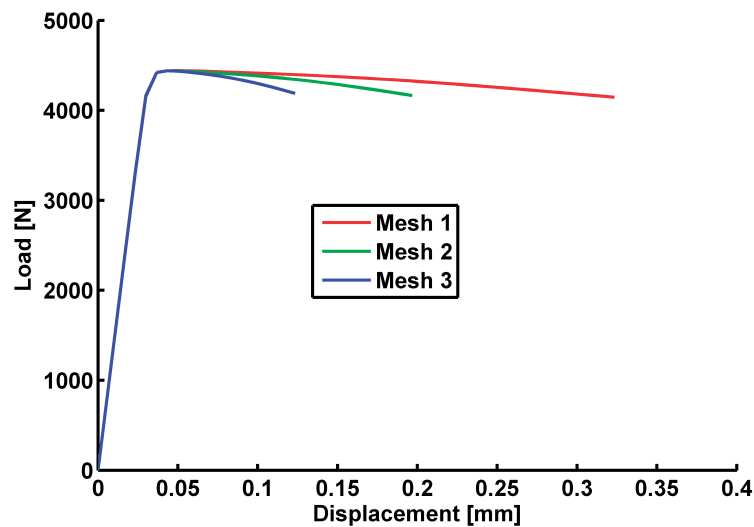


Figure 7: Response of a G-T-N material and an initial void content of 4%- QMITC Standard

The sample dimension is defined with  $L = 8\text{mm}$  and the loading process is developed imposing a uniform displacement on the upper boundary. The analyses are interrupted if  ${}^t\sigma_y$  plummets below 10% of initial  ${}^0\sigma_y$  or  ${}^t f$  grows beyond  $f_{critical}$ . The three mesh densities, listed in Table 1, are analyzed. Material parameters are:  $E = 200\text{GPa}$ ,  $\nu = 0.3$  and  $\sigma_y = 600\text{MPa}$ . The hardening exponent is set to  $N = 0$ , according to the results obtained in Fig. 1, aiming to trigger the localization while the small displacements hypothesis is still valid.

As a reference we plot the results obtained with standard QMITC elements and an initial void volume fraction of  ${}^0f = 0.04$  in Fig. 7. The void volume fraction and the equivalent plastic strain for mesh 3 are shown in Fig. 8. There, the shear band formation can be seen in the

Mesh	Horizontal Elem.	Vertical Elem.	Total Elem.
1	8	12	95
2	16	24	380
3	32	48	1520

Table 1: Regular meshes used to analyze the simple traction of a rectangular notched sheet

equivalent plastic strain and void content plots. Also mesh dependency is observed in the load displacement curve.

The results obtained using the new formulation are shown in Figs. 9 and 10 for  $^0f = 0.0$  and  $^0f = 0.04$  respectively. The void volume fraction and the equivalent plastic strain for mesh 3 and both initial void distributions are shown in Figs. 11 and 12. The mesh independency is evident from the load displacement plots. The difference in the triggering displacement is due to the initial void content. In the plotted meshes two different shear band paths are found, both being possible solutions.

For each  $h$ -value the results are almost mesh independent and the unloading slope is controlled by the lengthscale. Hence, an experimental technique for determining the lengthscale for different materials and microstructures is available. It is important to recognize that the lengthscale adoption implies that the energy is dissipated in an equivalent area,

$$h L = A_{localization}$$

defined by the  $h$ -parameter and, most important, that the parameter is not mesh dependent, that is to say, the parameter does need to be modified when using different element sizes.

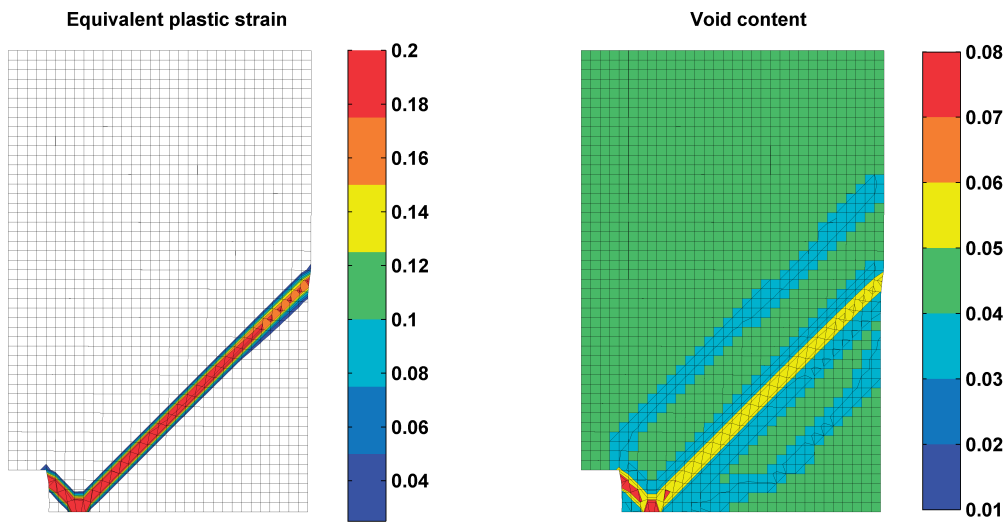


Figure 8: Equivalent plastic strain and void content for mesh 3 with 4% of initial void content - QMITC Standard

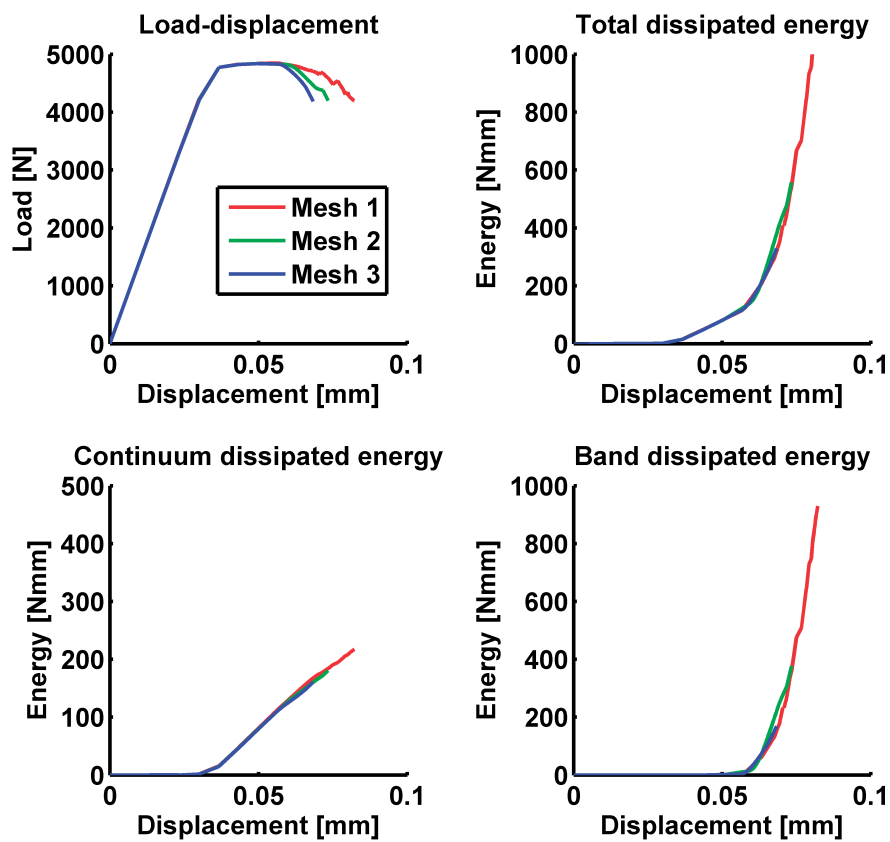


Figure 9: Response of a G-T-N material with lengthscale  $h=0.10\text{mm}$  and no initial voids - QMITC Localized

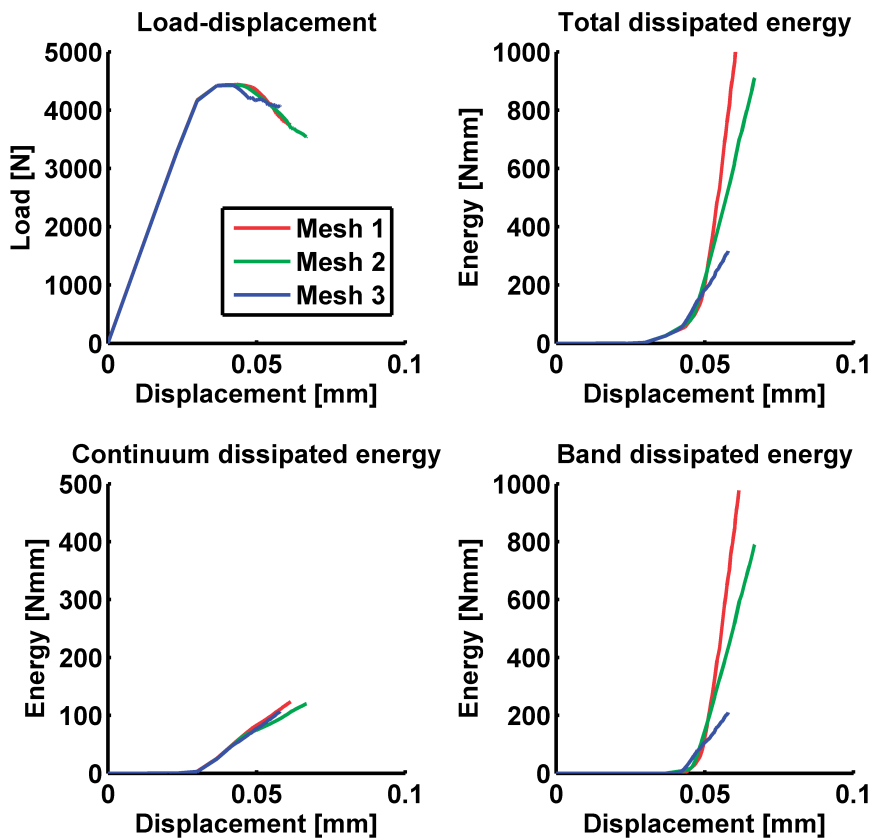


Figure 10: Response of a G-T-N material with lengthscale  $h=0.10\text{mm}$  and an initial void content of 4% - QMITC Localized

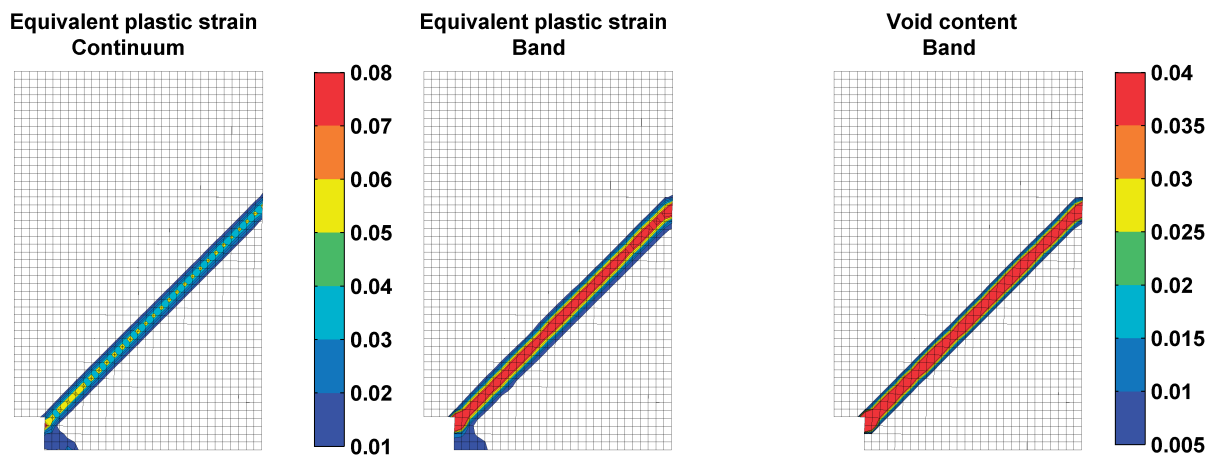


Figure 11: Equivalent plastic strain and void content for mesh 3 with no initial voids - QMITC Localized

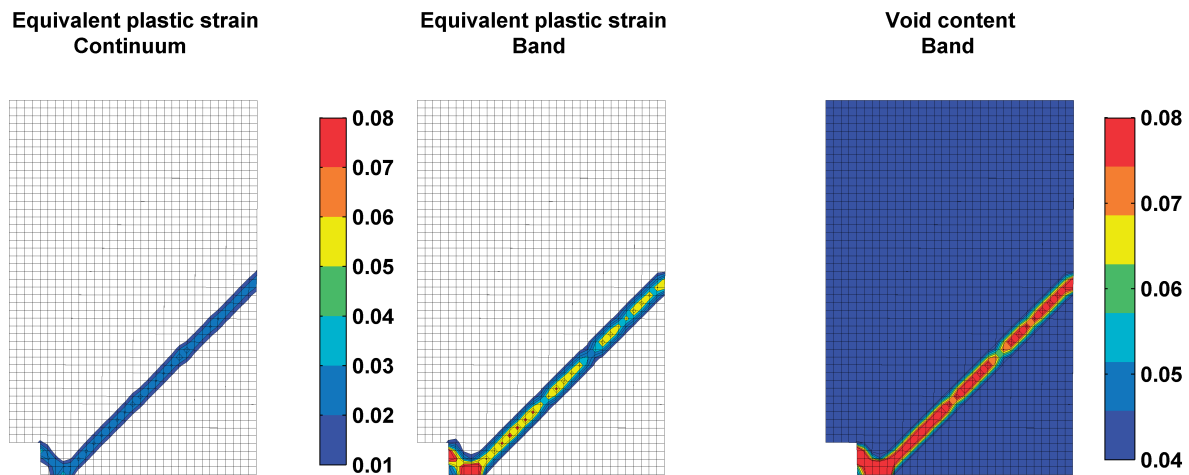


Figure 12: Equivalent plastic strain and void content for mesh 3 with 4% of initial voids - QMITC Localized

## 9 CONCLUSION

We extended the use of strong discontinuity modes to modeling strain localization phenomena in the G-T-N material. The localization scale is introduced into the finite element formulation embedding a strong discontinuity enhancement into the displacement field. The required inter-scales connection is achieved using an equivalent dissipated work criteria.

The heuristic introduction of the lengthscale parameter ( $h$ -parameter) allows to model the G-T-N material evolution inside the band. This  $h$ -parameter controls the unloading behavior and therefore it can be determined from actual experimental data. The resulting formulation provides mesh independent results and allows to control of the downslope part of the load-displacement path.

The necessary and sufficient conditions for the localization inception have been found.

**Acknowledgement:** Financial support has been received for this research from TENARIS and ITBA.

## REFERENCES

- Aravas N. "On the numerical integration of a class of pressure-dependent plasticity models.", *Int. J. Numerical Methods in Engng.*; **24**, pp. 1395-1416, 1987.
- Areias P. M. A. and Belytschko T., "Two-scale shear band evolution by local partition of unity", *Int. J. Numerical Methods in Engng.*, **66**, pp. 878-910, 2006.
- Armero F. and Garikipati K., "Analysis of Strong Discontinuities in Multiplicative Finite Strain Plasticity and Their Relation with the Numerical Simulation of Strain Localization in Solids", *Int. J. Solids and Structures*, **33**, pp. 2863-2885, 1996.
- Bathe K. J., *Finite Element Procedures*, Prentice Hall, New Jersey, 1996.
- Belytschko T., Loehnert S. and Song J. H., "Multiscale aggregating discontinuities: A method for circumventing loss of material stability", *Int. J. Numerical Methods in Engng.*, **73**, pp. 69-894, 2007.
- Chu C. C. , Needleman A., "Void nucleation effects in bi-axially stretched sheets", *J. Eng. Mater. Technol.*, **102**, pp. 249-256, 1980.
- D'heres S. and Dvorkin E. N., "Modeling shear bands in J2 plasticity using a two-scale formulation via embedded strong discontinuity modes", *Int. J. Numer. Meth. Engng*, **77**, pp.

- 1015–1043, 2009.
- D'heres S. and Dvorkin E.N., "On the modeling of shear bands formation in  $J_2$  materials with damage evolution", *Engng. Computations*, in press.
- Dvorkin E. N. and Vassolo S. I., "A quadrilateral 2D finite element based on mixed interpolation of tensorial components", *Engng. Computations*, **6**, pp. 217-224, 1989.
- Gurson A. L., "Plastic flow and fracture behavior of ductile materials incorporating void nucleation, growth and coalescence", Ph.D. thesis, Brown University, 1975.
- Gurson A. L., "Continuum theory of ductile rupture by void nucleation and growth: Part 1 - yield criteria and flow rules for porous ductile materials", *J. Eng. Matl. Tech.*, **99**, pp. 2-15, 1977.
- Koplik J. and Needleman A. "Void Growth And Coalescence in Porous Plastic Solids". *Int. J. Solids Structures*, **24**, pp. 835-853, 1988.
- Oliver J., "Modeling strong discontinuities in solid mechanics via strain softening constitutive equations. Part 1: Fundamentals", *Int. J. Numerical Methods in Engng.*, **39**, pp. 3575-3600, 1996.
- Oliver J., Cervera M. and Manzoli O., "Strong discontinuities and continuum plasticity models: the strong discontinuity approach", *International Journal of Plasticity*, **15**, pp. 319 –351, 1999.
- Oliver J. and Huespe A. E., "Theoretical and computational issues in modelling material failure in strong discontinuity scenarios", *Comput. Meth. Appl. Mech. Engng.*, **193**, pp. 2987-3014, 2004.
- Ortiz M., Leroy Y. and Needleman A., "A Finite-Element Method for Localized Failure Analysis", *Comput. Meth. Appl. Mech. Engng.*, **61**, pp. 189-214, 1987.
- Ottosen N. S. and Runesson K., "Properties of discontinuum bifurcation solutions in elastoplasticity". *Int. J. Solids Structures*, **27**, pp. 401-421, 1991.
- Rice J. R., "The Localization of Plastic Deformation", in *Theoretical and Applied Mechanics* (Proceedings of the 14th International Congress on Theoretical and Applied Mechanics, Delft, 1976, ed. W.T. Koiter), Vol. 1, North-Holland Publishing Co., pp. 207-220, 1976.
- Samaniego E. and Belytschko T., "Continuum–discontinuum modelling of shear bands", *Int. J. Numerical Methods in Engng.*, **62**, pp. 1857-1872, 2005.
- Sánchez P. J., Huespe A. E. and Oliver J., "On some topics for the numerical simulation of ductile fracture", *International Journal of Plasticity*, **24**, pp. 1008–1038, 2008.
- Simo J., Oliver J. and Armero F., "An analysis of strong discontinuities induced by strain-softening in rateindependent inelastic solids", *Computational Mechanics*, **12**, pp. 277–296. 1993.
- Sluys L. J., "Discontinuous modeling of shear banding", *Proc. Computational Plasticity COM-PLAS V*, (Ed. by D.R.J Owen, E. Oñate and E. Hinton), Barcelona, 1997.
- Tvergaard V., "Influence of voids on shear band instabilities under plane strain conditions", *Int. J. Fract.*, **17**, pp. 389–407, 1981.
- Tvergaard V., "On localization in ductile materials containing spherical voids", *Int. J. Fract.*, **18**, pp. 237–252, 1982.
- Tvergaard V. and Needleman, A., "Analysis of the cup-cone fracture in a round tensile bar", *Acta Metall.* **32**, pp. 157–169, 1984.
- Tvergaard V., Needleman A. and Lo K. K., "Flow localization in the plane strain tensile test", *Journal of the Mechanics and Physics of Solids*, **29**, pp. 115-142, 1981.
- Zhang Z. L., Niemi E., "A class of generalized mid-point algorithms for the Gurson-Tvergaard material model." *Int J Numer Methods Eng*, **38**, pp. 2033–2053, 1995.